CONDENSED MATTER PHYSICS

Original article
DOI: https://doi.org/10.18721/JPM.15401

THE DIELECTRIC RESPONSE MODIFICATION OF NANOCRYSTALLINE VANADIUM DIOXIDE FILMS BY DOPING WITH NICKEL AND TUNGSTEN

E. B. Shadrin[1]✉, *A. V. Ilinskiy*[1], *R. A. Castro*[2], *V. M. Kapralova*[3], *A. A. Kononov*[2], *M. E. Pashkevich*[3]

[1] Ioffe Institute of the Russian Academy of Sciences, St. Petersburg, Russia;

[2] Herzen State Pedagogical University of Russia, St. Petersburg, Russia;

[3] Peter the Great St. Petersburg Polytechnic University, St. Petersburg, Russia

✉ jenjasha@yandex.ru

Abstract. The process and salient features of modifying the structure of dielectric nanocrystalline vanadium dioxide films by doping with Ni and W transition metals have been studied. The dielectric spectra obtained experimentally were interpreted in terms of Debye relaxation theory and the equivalent circuit method. The changes in the spectra of doped compounds were established to be due to the selective effect of the dopants on various morphological structures of the film surfaces. It was shown that dielectric spectroscopy made it possible to obtain detailed information about parameters of relaxation response of different-sized morphological structures of films, and such information could not be extracted by other research methods.

Keywords: dielectric spectroscopy, vanadium dioxide films, VO_2, insulator-metal phase transition, correlation effects

Funding: The reported study was funded by Russian Foundation for Basic Research (grant No. 20-07-00730, “Dielectric spectroscopy of nanocrystalline vanadium oxide films doped with transition metals as basic elements of optical memory systems”).

For citation: Shadrin E. B., Ilinskiy A. V., Castro R. A., Kapralova V. M., Kononov A. A., Pashkevich M. E., The dielectric response modification of nanocrystalline vanadium dioxide films by doping with nickel and tungsten, St. Petersburg State Polytechnical University Journal. Physics and Mathematics. 15 (4) (2022) 7–31. DOI: https://doi.org/10.18721/JPM.15401

This is an open access article under the CC BY-NC 4.0 license (https://creativecommons.org/licenses/by-nc/4.0/)

© Shadrin E. B., Ilinskiy A. V., Castro R. A., Kapralova V. M., Kononov A. A., Pashkevich M. E., 2022. Published by Peter the Great St. Petersburg Polytechnic University.

Научная статья
УДК 537.876.4
DOI: https://doi.org/10.18721/JPM.15401

МОДИФИКАЦИЯ ДИЭЛЕКТРИЧЕСКОГО ОТКЛИКА НАНОКРИСТАЛЛИЧЕСКИХ ПЛЕНОК ДИОКСИДА ВАНАДИЯ ПУТЕМ ЛЕГИРОВАНИЯ НИКЕЛЕМ И ВОЛЬФРАМОМ

Е. Б. Шадрин[1]✉, *А. В. Ильинский*[1], *Р. А. Кастро*[2],
В. М. Капралова[3], *А. А. Кононов*[2], *М. Э. Пашкевич*[3]

[1] Физико-технический институт им. А. Ф. Иоффе РАН, Санкт-Петербург, Россия;

[2] Российский государственный педагогический университет им. А. И. Герцена, Санкт-Петербург, Россия;

[3] Санкт-Петербургский политехнический университет Петра Великого, Санкт-Петербург, Россия

✉ jenjasha@yandex.ru

Аннотация. Изучены особенности процесса модификации диэлектрическтого отклика нанокристаллических пленок диоксида ванадия при их легировании переходными металлами Ni и W. Интерпретация экспериментальных диэлектрических спектров проведена на основе теории релаксации Дебая и метода эквивалентных схем. Установлено, что изменения в диэлектрических спектрах легированных пленок VO_2 обусловлены селективным воздействием допантов на различные морфологические структуры поверхности пленок. Показано, что диэлектрическая спектроскопия позволяет получать детальную информацию о параметрах релаксационного отклика разноразмерных морфологических поверхностных структур, недоступную другим методам исследования.

Ключевые слова: диэлектрическая спектроскопия, пленка диоксида ванадия, фазовый переход полупроводник – металл, корреляционный эффект

Финансирование: Исследование выполнено при финансовой поддержке Российского фонда фундаментальных исследований (грант № 20-07-00730 «Диэлектрическая спектроскопия легированных переходными металлами нанокристаллических пленок оксидов ванадия – базовых элементов систем оптической памяти»).

Для цитирования: Шадрин Е. Б., Ильинский А. В., Кастро Р. А., Капралова В. М., Кононов А. А., Пашкевич М. Э. Модификация диэлектрического отклика нанокристаллических пленок диоксида ванадия путем легирования никелем и вольфрамом // Научно-технические ведомости СПбГПУ. Физико-математические науки. 2022. Т. 15. № 4. С. 7–31. DOI: https://doi.org/10.18721/JPM.15401

Статья открытого доступа, распространяемая по лицензии CC BY-NC 4.0 (https://creativecommons.org/licenses/by-nc/4.0/)

© Шадрин Е. Б., Ильинский А. В., Кастро Р. А., Капралова В. М., Кононов А. А., Пашкевич М. Э., 2022. Издатель: Санкт-Петербургский политехнический университет Петра Великого.

Introduction

Dielectric spectroscopy (DS), being a method of obtaining and analyzing the frequency response of a system to an external electric field, is a part of low and ultra-low frequency (10^{-3}–10^{6} Hz) impedance spectroscopy [1]. The most informative characteristic obtained by the DC method is the frequency dependence of the dissipation factor $\mathrm{tg}\delta(f) = \varepsilon''/\varepsilon'$, which is the ratio of the components of the complex permittivity $\varepsilon^* = \varepsilon' + i\varepsilon''$.

When an external electric voltage is applied, the bias current flowing through the ideal dielectric is ahead of the applied voltage in phase by an angle of $\psi = \pi/2$, and for a non-ideal dielectric $\psi = \pi/(2 - \delta)$ (δ characterizes the irreversible energy loss in the response process). The smaller the angle δ (and $\mathrm{tg}\delta$), the higher the quality of the dielectric with respect to its use in applications.

Along with their applications, DC methods are also actively used to obtain scientific information about the physical parameters of film materials, with the development of first-class dielectric spectrometers of record sensitivity.

This determined the purpose of this paper, which was to investigate thin oxide films of a highly correlated metal such as vanadium. DS enables selective detection of physical parameters of the semiconductor-metal phase transition (PT) mechanism in sharply different in size aggregates of VO_2 film nanocrystallites whose elements are randomly mixed on the substrate surface. No other method of study is capable of solving the problem of such selective sensing.

We remind that thermal PT in vanadium dioxide films occurs at $T = 340$ K, has a complex nature [2, 3] and allows efficient control of the transition characteristics by doping VO_2 films with transition elements, in particular Cr, Fe, Ni, and W. The effectiveness of the control is due not only to the modification of the numerical values of the PT parameters during doping, but also to the possibility of controlling the very complex nature of its performance.

This paper presents the results of a study of VO_2 films doped with both Ni and W.

1. Experimental methods

The samples studied were thin (100 nm) nanocrystalline films of vanadium dioxide synthesized by laser ablation technology on insulating substrates of varying thickness *d*. The specific feature of the method was a droplet mode of metal deposition on the substrate, in which two synchronous laser pulses excited metal particle torches, knocked out of two identical vanadium (V) targets, deposited a system of liquid metal droplets on the substrate heated to 500–700 °C.

The droplet sizes were distributed according to Gaussian law, and their oxidation occurred in a low-pressure oxygen stream ($4 \cdot 10^{-2}$ mm Hg) purged along the substrate surface. The parameters of the Gaussian distributions (position of maxima, half-widths) were controllable and for both targets could coincide or not with each other, depending on the ratio of the parameters of the bombarding laser pulses. If it was necessary to introduce a dopant into VO_2, we replaced one of the V targets by a transition metal (nickel or tungsten) target.

To control film morphology, we used an atomic force microscope (AFM-microscope) to obtain images of the film surface with a resolution of 10 nm and histograms of nanocrystallite size distribution.

The dielectric spectrometer measured the amplitude of voltage fluctuations on the reference resistor connected in series with the sample and the phase shift between the reference voltage and the voltage on the reference resistor. The converter transformed the parameters of measured voltages into the amplitude of alternating current flowing through the sample and into the value of phase shift between the applied voltage and the first harmonic of total current. The spectrometer computer generated dielectric spectra of the sample based on these data.

An empty measuring cell had an electrical capacity of $C_0 = \varepsilon_0 S/d$, where S is the area of the electrodes. An alternating sinusoidal voltage was applied to the electrodes

$$U(t) = U_0 \sin(\omega t) = \mathrm{Im}\,[U^* \exp(i\omega t)],$$

where U_0, ω are voltage amplitude and frequency, respectively, t is time.

If there was a test sample in the cell, a current flowed through it

$$I(t) = I_0 \sin(\omega t + \psi) = \mathrm{Im}\,[I^* \exp(i\omega t)] = \mathrm{Im}\,[I_0 \exp(i\psi) \exp(i\omega t)],$$

where ψ is phase shift with respect to the phase of the applied voltage oscillations.

Here, $U^* = U_0$, $I^* = I_0 \exp(i\psi) = I_0 \cos\psi + iI_0 \sin\psi = I' + iI''$.

Thus, in the DS method, U_0 was measured and the functions $I_0(f)$ and $\psi(f)$ were determined, on the basis of which the computer, according to the standard procedure, obtained dielectric spectra.

The dielectric spectra include:

$$–\varepsilon'(f) = I_0[\mathrm{tg}\psi(f)][1 + \mathrm{tg}^2\psi(f)]^{-1/2}(\omega C_0U_0)^{-1};$$

$$–\varepsilon''(f) = I_0[1 + \mathrm{tg}^2\psi(f)]^{-1/2}(\omega C_0U_0)^{-1};$$

$$–\mathrm{tg}\,\delta(f) = \varepsilon''/\varepsilon';$$

$$– Z'(f), Z''(f)$$

(Z^* is the complex impedance of the sample, $Z^* = Z' + iZ''$).

2. Experimental results and their interpretation

Preliminary remarks. The substrate temperature in the synthesis of vanadium dioxide was maintained in the range of 500–700 °C, which provided a high rate of movement of vanadium ions and oxygen on the substrate surface and high oxidative capacity of the metal in the flow of oxygen blown along the surface of the substrate. Automatic compliance with the condition of minimum thermodynamic potential at high ion mobility ensured, first, the correct stoichiometry within the volume of vanadium dioxide crystallites and, second, resulted in saturation of the nanocrystallite surface with metallic vanadium. The more effective the surface metallization was, the smaller was the radius of curvature of the nanocrystallite surface, since metallization led to a sharp decrease in the surface tension energy of the crystal. A common physical reason for minimizing surface energy during metallization is the fact that the surface tension energy density of a nanocrystallite is inversely proportional to the square of the radius of curvature of its surface. More specifically, metals have the property (unlike covalent and ionic compounds) that a relatively small number of their conduction electrons binds a much larger number of their ions into a single crystal lattice. Such a chemical bond with a deficit of electrons [4, 5] is characterized by an energy that is 5 to 10 times lower than the energy of a standard two-electron ionic or covalent bond. If we replace one of the vanadium targets with another transition metal target, such as nickel target (but not tungsten target), the surface energy reduction is even more effective, because in this case the dopant more actively saturates the surface of the nanocrystallite. This occurs according to the principle that in the near-surface layer of the crystallite, the component of the solid solution that has two-electron bonds with the matrix (in the presence of high ion mobility) that more strongly lowers the surface tension of the crystallite prevails [6]. The fact is that, according to the Pauling mechanism [7], the chemical bonds of those impurities, whose orbitals are more strongly shielded by the inner electron shells, have a lower energy (excluding multi-electron metallic bonds, where the situation is the opposite). The periodic table of chemical elements indicates that the degree of shielding by the inner electron shells is greater the higher the order number of the element. For dopants introduced into vanadium dioxide, the ordinal numbers are arranged in the following increasing order (by degree of shielding):

V, Cr, Fe, Ni, W.

The metallic bonding energy is also influenced (although slightly) by the coordination number of the metal ion. In our case, this influence should not be considered significant.

The presented brief analysis shows that at the same concentration of the doping additives, those that more effectively minimize the surface tension energy will appear on the surface of smaller nanocrystallites with greater curvature.

A comparison of the parameters relevant to our case is given in Table 1 (values for vanadium are in bold).

Table 1

Physical and chemical parameter values of the metals concerned

Metal	Melting temperature, °C	Bond energy, kJ/mole	Conductivity, MS/m
Al	660	120	37
Cr	1907	380	9
Fe	1538	430	10
Ni	1455	430	14
V	**1910**	**520**	**15**
W	3422	850	19

The tungsten atom W, which stands alone as a donor in the VO_2 crystal (Al is the acceptor), has a very high metallic bonding energy and, consequently, a high melting point, draws attention. Although doping with this element lowers the PT temperature (this will be shown below in Section 2.4), it does not lower the surface energy of the nanocrystal because tungsten does not reach the surface of the nanocrystal due to its higher metallic bonding energy than that of the vanadium atom. The point is that the stronger the metal bond, the greater the density of the free electron gas (conduction electrons) in which the ions of the metal's crystal frame are immersed. The electrical conductivity of tungsten is several times higher than that of vanadium, which determines the high strength of tungsten metal bonding.

It should be noted that the martensitic nature of the structural (Peierls's) part of the complex semiconductor-metal PT in vanadium dioxide film nanocrystallites additionally modifies those parameters of the thermal hysteresis loops of the frequency position of the DC peaks, which are caused by the presence of impurity. Different impurities differently lower the surface tension energy of the film grains and thus differently metallize the surface of nanocrystallites of different sizes, which is reflected in the values of the widths of the corresponding thermal hysteresis loops. This is because the width of the thermal hysteresis loop is inversely proportional to the square root of the grain cross section due to the martensitic nature of the transition [8].

Finally, let us point out that the DS method solves the problem of plotting the $G(\tau)$ distribution of the relaxation response times of nanocrystallites over their values in ultrathin (50 nm) vanadium dioxide layers, even in the presence of an extremely wide range of relaxation times.

The function $G(\tau)$ is a time-dependent differential distribution function of the "time" density of relaxators $dN/d\tau$, i.e., the number of relaxators per unit time interval. The integral of such a function with an infinite upper limit is equal to the total number of relaxators. In our case of domination of processes of drift of conduction electrons at shielding of a field it appears that after application of an external electric field time of relaxation is time of formation of stationary concentration of free electrons in the area of a spatial charge.

This paper presents the experimental results obtained in the study of thin nanocrystalline films of strongly correlated vanadium dioxide by the DS method. Both specially undoped vanadium dioxide films and vanadium dioxide films doped with nickel and tungsten were the objects of the study.

2.1. Undoped VO_2 film with unimodal nanocrystallite size distribution

The dielectric spectra of an undoped vanadium dioxide film are shown in Fig. 1, *a*, *b* as frequency dependences of the real (ε) and imaginary (ε) parts of the dielectric permittivity measured at room temperature $T = 293$ K. Comparison of the experimental and calculated data is presented. Frequency dependences of dielectric permittivity components were calculated by equation (1) (Fig. 1, *a*, *b*). They contain one step on the graph of the function $\varepsilon'(f)$ and one maximum on the graph of the function $\varepsilon''(f)$. The step and maximum are located at a frequency of 0.1 MHz.

These spectra are presented, in addition, as a frequency dependence of the dielectric loss tangent tgδ(f) and the Cole–Cole diagram (CC), i.e., ε″(ε′) (Fig. 1, *c*, *d*). The calculation in this case is made by equations (3) and (4). Frequency dependence of tgδ(f) contains, as well as dependence ε″(f), one maximum, and the diagram contains one semicircle. The following indicates the standard distribution of film nanocrystallites by their size, close to the Gaussian distribution in shape: the presence of one maximum in the functions ε″(f) and tgδ(f), one semicircle of 'correct' form on the CC diagram, as well as one maximum on the curve of film grain size distribution, which was obtained in the analysis of the atomic force image of the film surface.

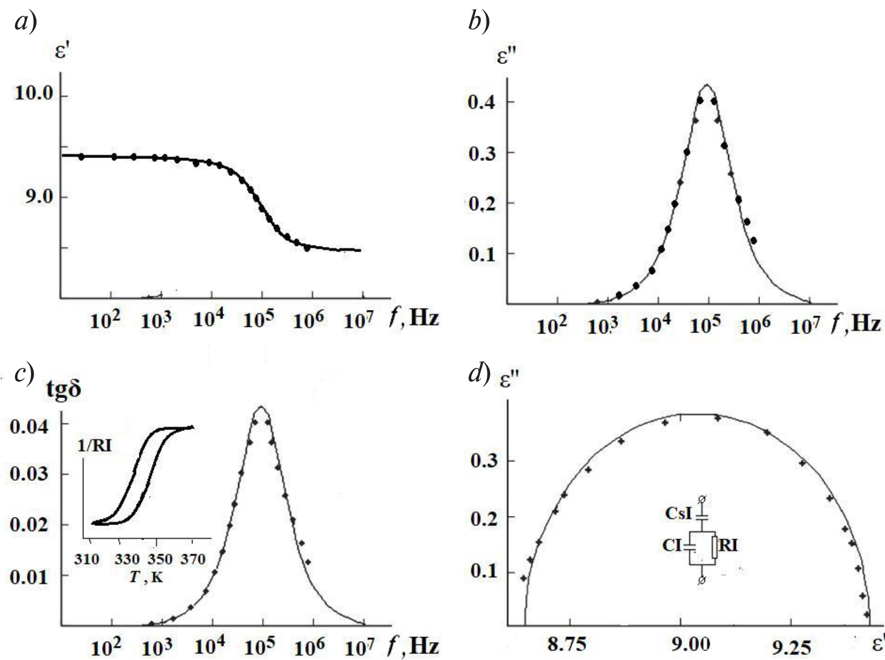

Fig. 1. Experimental (dots) and calculated (lines) frequency dependences of the real (*a*) and imaginary (*b*) parts of the dielectric permittivity, the dissipation factor (*c*), and the Cole–Cole diagram (*d*) for a homogeneous undoped VO_2 film at T = 293 K.
The box to Fig. 1,*c* shows the temperature hysteresis loop of the frequency position of the maximum tgδ(f) and the associated film conductivity 1/*RI*.
The inset to Fig. 1,*d* shows a single-circuit equivalent electrical scheme

2.1.1. Analysis of experimental results

We analyzed the measurement results from the Debye theory and calculations of the parameters of electrical equivalent circuits of aggregates of nanocrystalline grains of the studied samples. The physical meaning of the circuit elements is described later in this section.

Analysis in terms of Debye's relaxation theory. This classical theory [9] suggests the presence of one type of relaxants with a single relaxation time τ in the material under study. The situation in this case has a mechanical analogue in the form of a weight on a spring with a single frequency of natural vibrations, placed in a liquid medium, which provides losses of mechanical energy due to friction. In both cases, the distribution of relaxation times is a delta function, whereas the parameters reflecting the frequency dependence of the system's response to an external periodic influence (the amplitude of the weight oscillations, the imaginary part of the dielectric permittivity, and the tangent of the dielectric loss angle) have extended frequency peaks of nonzero half-width.

For a vanadium dioxide film, the complex permittivity, reflecting the response of a set of nanocrystallites to an external periodic electric field, is

$$\varepsilon^*(\omega) = \varepsilon' + i\varepsilon'',$$

where

$$\varepsilon'(\omega) = \varepsilon_\infty + \Delta\varepsilon/[1 + (\omega\tau)^2],\ \varepsilon''(\omega) = \Delta\varepsilon\cdot\omega\tau/[1 + (\omega\tau)^2].$$

If we write it down in a more compact form, we get the following equality:

$$\varepsilon'(\omega) = \varepsilon_\infty + \frac{\Delta\varepsilon}{1-(i\omega\tau)}, \tag{1}$$

where ε_∞ is high-frequency limit of the real part of the complex permittivity ε^*, $\Delta\varepsilon$ is dielectric increment (the difference between the low-frequency and high-frequency limits of the actual parts of the dielectric permittivity), $\omega = 2\pi f$ is cyclic frequency.

According to expression (1), the real part $\varepsilon'(f)$ has one step, dielectric loss function $\varepsilon''(f)$ and function tg$\delta(f)$ have one maximum at frequency $f = 1/(2\pi\tau)$. CC diagram $\varepsilon''(\varepsilon')$ in this case is a regular semicircle, the center of which is located on the abscissa axis. In our case, the results of calculation by formula (1) approximate well the experimental data (see Fig. 1, *a*, *b*) for the VO_2 film with a single maximum on the crystallite size distribution (with unimodal distribution).

However, in many cases a good agreement with the experiment cannot be achieved by the method described above, since one type of relaxers has a set of different, but close in value, relaxation times. The distribution of relaxation times according to their values appears in the experimental CC diagrams as a distortion of the half-circle shape and lowering of its center below the abscissa axis. The article [10] describes a special method for taking into account the differences between the experimentally measured dielectric spectra and the appearance of the corresponding spectra given by Debye's relaxation theory. For this purpose, the function $G(\tau)$ of the relaxation time distribution density is introduced into consideration, according to the expression [11]:

$$\varepsilon^*(\omega) = \varepsilon_\infty + (\varepsilon_s - \varepsilon_\infty)\int_0^\infty \frac{G(\tau)}{1+i\omega\tau}d\tau. \tag{2}$$

The Havriliak–Negami function [11], which contains three varying parameters: τ_{HN}, α_{HN}, and β_{HN}, can be used as such a 'correction' function. After a good agreement of the calculation results with the dielectric measurement data is achieved at fitting, one can judge the width, asymmetry, and position of the maximum of the $G(\tau)$ function by the values of these parameters. In the limiting case, when all relaxants of a given type have the same relaxation time τ, the function $G(\tau)$ turns into a δ-function. For the analyzed case of films with Gaussian grain size distribution, a variant of a narrow and symmetric function $G(\tau)$ is realized, as evidenced by the correct shape of the circle of the CC diagram with the center located on the abscissa axis.

Analysis based on the method of equivalent circuits. In the case of the analysis of the results for the VO_2 film with unimodal grain size distribution (see Fig. 1, *c, d*), the equivalent scheme of the sample is presented in the inset in Fig. 1, *d*. The physical meaning of the circuit elements is as follows: the capacitance C_sI is the electrical capacitance of the insulating substrate, CI is the electrical capacitance of the VO_2 film, and RI is the film ohmic resistance. Such one-loop circuit corresponds to one type of relaxers with a single relaxation time, i.e. it corresponds to Debye's theory (see formula (1)).

Calculation of the parameters of equivalent circuits is performed by the symbolic method. Calculation of the complex impedance $Z^* = Z' + iZ''$ of the single-loop circuit gives expressions:

$$Z' = \frac{R\mathrm{I}}{(\omega C\mathrm{I}R\mathrm{I})^2 + 1}, \quad Z'' = \frac{\omega^2 R\mathrm{I}^2 C\mathrm{I}\left(C\mathrm{I} + C_s\mathrm{I}\right) + 1}{\omega C_s\mathrm{I}\left(\omega^2 C\mathrm{I}^2 R\mathrm{I}^2 + 1\right)},$$

After the corresponding transformations we have the expressions

$$\mathrm{tg}\delta = \frac{R\mathrm{I}\omega C_s\mathrm{I}}{1 + R\mathrm{I}^2\omega^2 C\mathrm{I}\left(C\mathrm{I} + C_s\mathrm{I}\right)}, \tag{3}$$

$$\varepsilon'' = \sqrt{\frac{\varepsilon' C_s\mathrm{I}\left(2C\mathrm{I} + C_s\mathrm{I}\right)}{C\mathrm{I}\left(C\mathrm{I} + C_s\mathrm{I}\right)}\left(\varepsilon'\right)^2 - \frac{C\mathrm{I}C_s\mathrm{I}^2}{\left(C\mathrm{I} + C_s\mathrm{I}\right)C_0^2}}. \tag{4}$$

In expression (4), the parameter ω is excluded, and the function $\varepsilon''(\varepsilon')$ itself describes a semicircle with two points of intersection of the abscissa axis (roots) and is a Cole−Cole diagram. The first (right) root $\varepsilon' = C_s\mathrm{I}/C_0$ corresponds to the limit at $\omega \to 0$ and represents the low-frequency root of the function $\varepsilon''(\varepsilon')$ in the CC diagram (right root in Fig. 1,*b*). The second (left) root $\varepsilon' = C\mathrm{I}C_s\mathrm{I}/(C\mathrm{I} + C_s\mathrm{I})C_0$ corresponds to the limit at $\omega \to \infty$ and represents the high-frequency root of the function $\varepsilon''(\varepsilon')$ in the CC diagram (left root in Fig. 1,*d*). The radius of the half-circle h is equal to the half-difference of the roots of the function $\varepsilon''(\varepsilon')$, i.e.,

$$h = \frac{C_s\mathrm{I}^2}{2\left(C\mathrm{I} + C_s\mathrm{I}\right)C_0}.$$

The analytical expression of the function $\varepsilon''(\varepsilon')$ shows that the CC-diagram parameters depend only on the electric capacities $C_s\mathrm{I}$ and $C\mathrm{I}$ and do not depend on the value of electrical resistance RI. At the same time the function $\mathrm{tg}\delta(f)$ has a maximum at the frequency determined by both $C_s\mathrm{I}$ and $C\mathrm{I}$ and R values:

$$f_0 = \frac{1}{2\pi R\mathrm{I}C\mathrm{I}\sqrt{\frac{C_s\mathrm{I}}{C\mathrm{I}} + 1}}. \tag{5}$$

The single loop equivalent circuit allows a good agreement of the calculation results with the experiment at the following circuit parameters:

$$R1 = 1.2 \text{ kOhm}, \; C_s1 = 200 \text{ pF}, \; C1 = 1400 \text{ pF}.$$

It follows from expression (5) that the frequency at which the maximum of the $\mathrm{tg}\delta(f)$ function is located is directly proportional to the film conductivity $1/R\mathrm{I}$, and the characteristic relaxation time depends only on the film parameters $R\mathrm{I}$ and $C\mathrm{I}$:

$$\tau = R\mathrm{I}\cdot C\mathrm{I}\cdot[(C_s\mathrm{I}/C\mathrm{I}) + 1]^{1/2} \approx R\mathrm{I}\cdot C\mathrm{I}\cdot(C_s\mathrm{I}/C\mathrm{I} = \varepsilon_s\mathrm{I}d\mathrm{I}/\varepsilon\mathrm{I}d_s\mathrm{I} << 1).$$

The accepted approximation is quite valid because of the large difference between the thicknesses of the film and the substrate, which is at least four orders of magnitude.

As the experiment shows, the frequency f_0, at which the maximum $\mathrm{tg}\delta(f)$ is located, shifts towards high frequencies when the temperature increases, and when the temperature decreases

towards low frequencies. According to expression $f_0 \approx 1/(R\text{I} \cdot C\text{I})$, the shift in frequency is caused only by thermal change of conductivity $1/R\text{I}$ of the film, as film electrical capacity, judging by temperature constancy of experimental value

$$h = \frac{C_s \text{I}^2}{2\left(C\text{I} + C_s\text{I}\right)C_0} \tag{5}$$

does not depend on temperature.

The experiment shows, in addition, that the temperature dependence of conductivity $1/R\text{I}$ demonstrates thermal hysteresis, the heating side of which loop (loop width 8 K) is located at T_C = 340 K (see inset in Fig. 1,*c*).

2.1.2. Interpretation of results obtained

We assume that the parameters of the dielectric spectra (frequency position of the $\varepsilon'(f)$ step, $\varepsilon''(f)$ and tg$\delta(f)$ maxima, and the shape of the CC diagram) are due to free conduction electrons. In this case the characteristic response time of the system to an external electromagnetic influence is the Maxwell relaxation time $\tau_M = \varepsilon\varepsilon_0/\sigma$ [12], which agrees with the simplest numerical estimate. At 293 K, i.e., far from the PT temperature (T_C = 340 K), the VO_2 film nanocrystallites are in semiconductor phase with low concentration of free electrons and consequently low electrical conductivity of the film. The Maxwell time is large and the maximum of the function tg$\delta(f)$ is in the low-frequency region (see Fig. 1) (the position of the maximum is determined by the product $RC = t_{max} = 1/2\pi f_{max}$). With increasing temperature the concentration of free electrons in the semiconductor phase and the specific conductivity of nanocrystallites increases, the t_M time decreases and the maximum tg$\delta(f)$ shifts towards high frequencies.

The presence of conduction hysteresis loop as well as its position on the temperature scale (see inset in Fig. 1,*c*) testifies to the occurrence of semiconductor-metal PT in VO_2 nanocrystals, which has a complex character and consists of Mott electronic transition and Peierls structural transition [3]. The Mott transition is due to strong electron-electron correlations, which leads to the dependence of the energy position of the zones on their electron population and to the replacement of the Fermi distribution with tails of 30 MeV at T = 300 K by the Migdal distribution with tails of 250 MeV [13].

At high temperatures ($T > T_C$) the crystal lattice of VO_2 has tetragonal symmetry in the metallic phase, with vanadium ions arranged in the centers of octahedral oxygen frameworks formed by

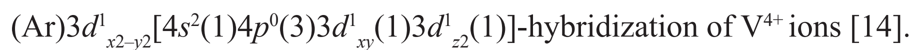

$$(\text{Ar})3d^1_{x2-y2}[4s^2(1)4p^0(3)3d^1_{xy}(1)3d^1_{z2}(1)]\text{-hybridization of } V^{4+} \text{ ions [14].}$$

As the temperature drops below the critical T_C = 340 K (67 °C), the crystal lattice decreases its symmetry from tetragonal to monoclinic by doubling the period along the rutile C_R axis, which leads to a gap in the energy spectrum with the formation of an upper ($3d_{top}$) and lower ($3d_{bott}$) Hubbard subzone [3]. The lower subzone plays the role of the valence band, while the conduction band, separated from the valence band by a 0.7 eV gap, is formed by the π^*-zone due to the π-bond of V_{dxz}–O_{pz} in the oxygen octahedron [3]. With decreasing temperature, due to the formation along the C_R axis of a chain of (V-V)-dimers [15], at T_C = 340 K a metal-semiconductor PT occurs which has thermal hysteresis due to the martensitic character of this phase transformation.

2.2. Undoped VO_2 film with bimodal nanocrystallite size distribution

2.2.1. Experimental results

Fig. 2 (T = 293 K) shows the frequency dependence of the imaginary part $\varepsilon''(f)$ of the complex permittivity and the CC diagram $\varepsilon''(\varepsilon')$ for this distribution. In this case two maxima of the function $\varepsilon''(f)$ and two semicircles in the CC diagram are observed. This suggests that there are two types of relaxers involved in the response of the system to an alternating electric field [14, 16].

We attribute the complicated appearance of the dielectric spectra and the presence of two types of relaxants to the bimodal size distribution of the synthesized VO_2 film nanocrystals.

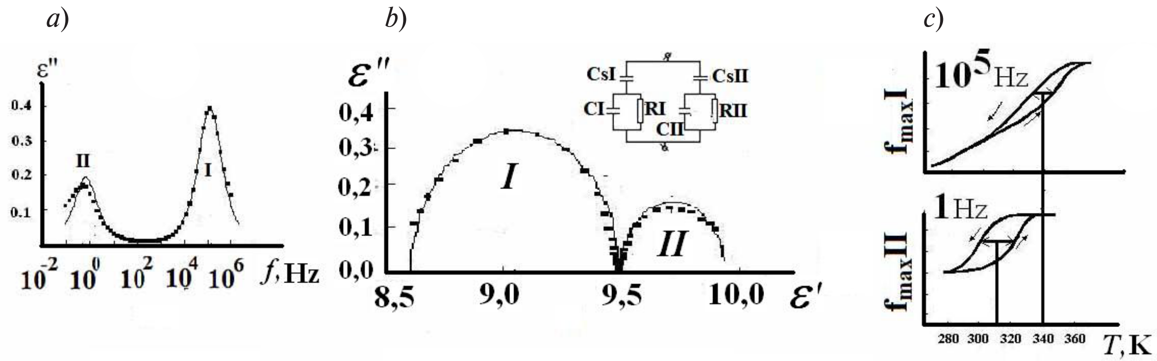

Fig. 2. Experimental (dots) and calculated (lines) frequency dependences
of imaginary part of complex permittivity (*a*), CC diagram (*b*) and hysteresis loops (*c*)
frequency positions of maximums of ε''(*f*) function
for heterogeneous undoped VO_2 film
T = 293 K. Calculation was carried out by equation (6)

2.2.2. Analysis of experimental results

The atomic force image and histogram of nanocrystallite size distribution demonstrate the presence of two types of nanocrystalline grains in the film: conventionally small and conventionally large. This was the reason for selecting the more complex Debye formula (6) and the two-loop version of the equivalent electrical circuit (inset in Fig. 2).

In this case, Debye's formula is as follows:

$$\varepsilon^*(\omega) = \varepsilon_\infty + \frac{\Delta\varepsilon_1}{1+i\omega\tau_1} + \frac{\Delta\varepsilon_2}{1+i\omega\tau_2}, \quad (6)$$

where $\Delta\varepsilon_1$, $\Delta\varepsilon_2$ are dielectric increments, $\Delta\varepsilon_1 = \varepsilon_s - \varepsilon_i$, $\Delta\varepsilon_2 = \varepsilon_i - \varepsilon_\infty$.

Formula (6) adequately describes the experimental spectra (Fig. 2, *a*, *b*) with fixed values $\tau_1 = 2\cdot10^{-6}$ s and $\tau_2 = 5\cdot10^{-2}$ s.

A two-loop equivalent circuit (inset in Fig. 2,c) is applicable to the analysis of dielectric spectra of the film with two types of relaxants determining the electrical response of the sample. The analytical expressions for the complex impedance of the circuit, which we obtained by the symbolic method, are very cumbersome and therefore not given in this paper. For standard computer programs, performing a fitting based on calculation results is not a difficult task. If the parameters of the equivalent circuit are chosen appropriately, they agree well with the measurement results.

The temperature dependences of the dielectric spectra carried out for a film with a bimodal size distribution of nanocrystallites show hysteresis loops for each maximum of ε''(*f*) (see Fig. 2,*c*). These loops differ in width and their position on the temperature scale. The loop width for maxima I is almost half that of maxima II. The position of the maximum II loop on the temperature scale is lower (T_C = 312 K) than that of maximum I (T_C = 342 K).

Interpretation of results. The interpretation is based on the fact that the differences in the loop parameters for different maxima are related to the martensitic character of PT in vanadium dioxide [17] and peculiarities of film synthesis by laser ablation [18] carried out at a substrate temperature of 700 °C. The difference in the frequency positions of the maxima, the widths of their hysteresis loops, and their positions on the temperature scale require explanation.

The explanation for the differences is based on the following considerations.

First, in small-sized nanocrystallites the surface contribution to the overall PT energy is dominant, in contrast to large-sized nanocrystallites.

Secondly, the condition of minimization of the thermodynamic potential dictates that the surface of the nanocrystallites must be metallized, which is ensured by the metallic vanadium of the parent material due to the sharply reduced metallic bond energy in vanadium as compared to

the ionic or covalent bond energy in non-metals (see Introduction). Reduction of surface energy by metallization is the more effective the higher the curvature of the crystallite surface is, i.e., the smaller its transverse size. The phenomenon of metallization of the surface of individual sets of film crystallites is well known from the literature [19].

Thirdly, the plume of metallic particles ejected by a laser pulse during film synthesis contains in general case conglomerates of particles whose sizes are distributed according to the law close to the Maxwell energy distribution of gas molecules. The minimum size is limited to values close to zero, while the maximum size is distributed in a long 'tail' with values many times larger than their value in the distribution maximum.

The conditions for the synthesis of nanocrystallites in the laser ablation method were chosen so that the size distribution of the synthesised nanocrystallites had two maxima, so that practically no medium-sized crystallites were formed. This was achieved by increasing the substrate temperature to 700 °C and by placing specially shaped screens in the path of the plume of vanadium metal particles knocked out by the laser pulse. Each distribution with its maximum had a shape close to a Gaussian distribution but with different Gaussian parameters. These measures caused that during the oxidation process in the oxygen stream the members of the family of small crystallites, actively covered with a metallic shell, almost immediately lost access of oxygen to their centres due to the metallization of the surfaces, whereas the metallization from the outside with vanadium atoms continued unimpeded. Due to the condition of electrical neutrality of the crystal, the subsurface layer of the crystal adjacent to the metallized layer from the inside was inevitably saturated with oxygen ions. At the same time there was an oxygen deficiency in the depth of the crystallite in the form of vacancies [20], as the oxygen flow from the outside was closed. The migration of oxygen ions, which ensured that the subsurface stoichiometry was maintained, was very effective because the ion mobility at 700 °C is very high. Oxygen vacancies in the depth of the crystallite, playing the role of electron donors, lowered the T_C temperature inside the grain due to the formation of small radius polarons with reduced ionization energy on them [21], while the metallization of the surface dramatically increased the electrical capacity of the metallized set of small crystallites. For these reasons, the low-frequency maximum $f_{max} = (1/R)(1/C)$ on the distribution curve for small grains has a wide hysteresis loop (martensite) with a reduced (due to donor influence) position of the hysteresis loop on the temperature scale.

Note that the effective electrical conductivity $1/R$ of metallized nanocrystallites is very low due to the lack of charge sinking channel from the surface of metallized particles. The charge outflow is hindered by the minimization factor of the surface tension energy due to the metallization of the surface. Namely, any increase in conductivity equivalent to the discharge from the surface of a metallic layer reduces the strength of the metallic bond in that layer, thereby violating its integrity, which must necessarily lead to the departure of the thermodynamic potential from the energy minimum [12]. The multipliers $1/R$ and $1/C$ determining the f_{max} position were therefore extremely small, so it follows that this maximum must be located at a low frequency, as observed in the experiment.

At the same time, the inside of metallized grains, saturated with oxygen vacancies (electron donors), retains the ability to perform thermal semiconductor-metal PT, and at reduced T_C temperature, which is also observed in experiment.

After occurrence of FP while heating the sample, the grains, metallized only on the surface, become entirely metallic; in this case the value of f_{max} increases, which is shown in the experiment by formation of an extended thermal branch of the hysteresis loop. Cooling, on the other hand, forms a cooling branch in the reverse process.

In order to perform a Peierls jump PT, a deviation from the T_C temperature is necessary, associated with the need to introduce additional thermal energy required to change the symmetry of the crystal lattice. The condition for the introduction of additional energy is determined by the need to overcome the excess Laplace pressure, generated by the surface tension of the crystallite and proportional to the curvature of the surface. The portion of additional energy, according to Laplace theorem, is proportional to the square root of the surface curvature of the nanocrystal.

Most often, the temperature of the heating branch of the hysteresis loop is taken as the T_C value of the Peierls structural transition in a first approximation. However, strictly speaking, for

this value, i.e. the *TC* temperature of equilibrium of the semiconductor and metallic phases, it is necessary to take the middle of the hysteresis loop, if the elementary loops composing the main loop are symmetrical about this T_C temperature point.

Thus, as a result of the dominant contribution of oxygen vacancies to the PT energy, the T_C value of highly defective small grains is reduced due to correlation effects, while the hysteresis loop width is increased due to the high curvature of the surface (small curvature radius), and the ε″ maximum is located in the low frequency region. All this is observed in the experiment (see Fig. 2, *a*, *c*).

2.3. Vanadium dioxide films doped with nickel

2.3.1. Experimental results

Fig. 3 shows results of dielectric measurements of frequency dependences of real (ε′) and imaginary (ε″) parts of complex dielectric permittivity ε* of vanadium dioxide film doped with nickel (VO_2 : Ni). The results have been obtained in the temperature range 293–373 K (20–100 °C). A Cole–Cole diagram ε″ (ε′) is also presented.

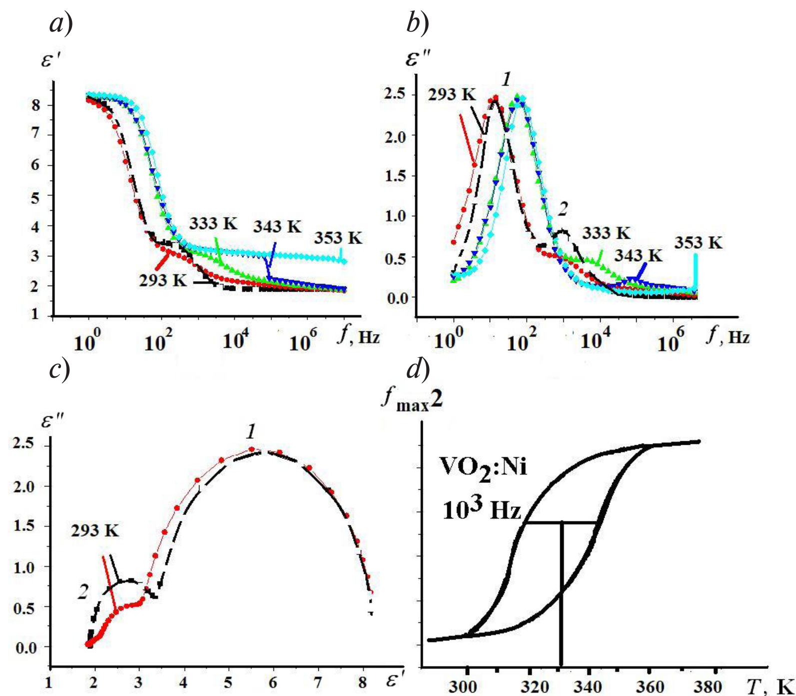

Fig. 3. Experimental (dots) and calculated (lines) frequency dependences of the real (*a*) and imaginary (*b*) parts of permittivity for VO_2 : Ni film at different temperatures, as well as the Cole–Cole diagram at T = 293 K; the calculation is based on formula (6)

For the maximum 2 (see Fig. 3, *b*) a hysteresis loop of its frequency position - 1 kHz is presented (*d*)

The comparison of the spectra in Fig. 3 with the spectra of the non-doped film shows that with nickel doping an additional maximum 2 appears in the dielectric spectra at high frequencies (approximately 1 kHz), which we identified as belonging to a separate population of grains doped with nickel. Note especially that the size distribution of the nanocrystallites has only one maximum.

The temperature dependence of the frequency position of the highest (main) maximum 1 of the function ε″(*f*) shows a thermal hysteresis with the heating branch of the loop located at T_C = 340 K (67 °C). The loop has the temperature width of 12 K. The geometric center of this

loop is located at 334 K (61 °C). This temperature can be taken, in accordance with the martensitic character of this phase transformation, as the equilibrium temperature of the semiconductor and metallic phases in the case of strictly symmetric elementary loops composing the main loop [17].

The hysteresis loop of the second, smaller maximum 2, located in the higher frequency region of the spectrum (f_2), is located at lower temperatures than the loop of the higher maximum. More specifically, its geometrical center, taken as the phase equilibrium temperature, is located at 331 K (58 °C). The width of the lower maximum loop is 28 K (Fig. 3,*d*).

The presence of temperature hysteresis loops testifies that the crystal grains of vanadium dioxide film undergo a phase transformation in the region of $T_C \approx 335{-}345$ K which is a semiconductor-metal PT for vanadium dioxide [3]. CC-diagram of VO_2 : Ni film, as well as dielectric spectra, after doping acquires an additional feature and contains instead of one two semicircles which parameters practically do not depend on temperature in the region $T \leq T_C$ (see Fig. 3,*c*).

2.3.2. Analysis of experimental results

Dielectric spectra and CC diagrams contain two features. Therefore, to calculate these spectra, formula (6) should be used, and when analyzing the results using the method of equivalent circuits, the two-loop version of the equivalent circuit should be chosen. When analyzing the experimental results, we took into account the following circumstances.

Circumstance 1. Although the dielectric spectra calculated by formula (6) correspond qualitatively to experiment, the reality is that the experimental spectra are more complex than the calculated ones. Namely, calculated curves $\varepsilon'(f)$, in comparison with experimental ones, have steeper steps, calculated $\varepsilon''(f)$ peaks appear narrower; the experimental CC diagram does not have a regular half-circle look like the diagram calculated according to formula (6), its half-circles have heights less than half their diameters. The point is that the VO_2 : Ni sample acquires at least two different types of relaxants as a result of doping, and each type receives a set of separate relaxants with close relaxation times, i.e., with a non-zero width of their time distribution. Different types of relaxers give several maxima of the function $\varepsilon''(f)$ and several semicircles in the CC diagram. In addition, a distortion of the shape of $\varepsilon''(f)$ curves and the shape of semicircles in the CC diagram appears. To account for these distortions we replaced formula (6) by formula (2) for each type of grain and introduced a refined function $G(\tau)$, a function of relaxation time density distribution over relaxation times. The Havriliak–Negami function [11] of the form (7) was used as such a function in the calculations. This function for each grain type contains three varying parameters (τ_{HN}, α_{HN} and β_{HN}) and has the following form:

$$G(\tau)=\frac{1}{\pi}\times\frac{(\tau/\tau_{HN})^{\beta(1-\alpha)}\sin(\beta\varphi)}{\left[(\tau/\tau_{HN})^{2(1-\alpha)}+2(\tau/\tau_{HN})^{(1-\alpha)}\cos(\pi[1-\alpha])+1\right]^{\beta/2}}, \quad (7)$$

where

$$\varphi=\operatorname{arctg}\left[\frac{\sin(\pi[1-\alpha])}{(\tau/\tau_{HN})+\cos(\pi[1-\alpha])}\right].$$

The distributions of relaxants over relaxation times are characterized by the parameters of the Havriliak–Negami (HN) function, which reflect the averaged position of relaxants on the timescale τ_{HN}, the degree of scatter α_{HN}, and the heterogeneity (asymmetry) β_{HN}. The software of modern spectrometers makes it possible to output the HN function with the values of the parameters τ_{HN}, α_{HN} and β_{HN} already adjusted to the measurement results. After achieving a good agreement between the calculation results according to formula (2) and measurement

data, the dielectric spectrometer outputted a graph of the relaxation time distribution function in the VO_2 : Ni film, shown in Fig. 4. There are two narrow ($\alpha_{HN1} \approx \alpha_{HN2} = 0.05$) and practically symmetric ($\beta_{HN1} \approx \beta_{HN2} = 0.97$) peaks. In our case (for dielectric spectra of semiconductor films), this indicates the closeness of the HN functions found by the spectrometer to δ-functions with characteristic times $\tau_{HN1} = 10^{-2}$ s and $\tau_{HN2} = 1.6 \cdot 10^{-4}$ s for unalloyed and nickel-doped grains, respectively.

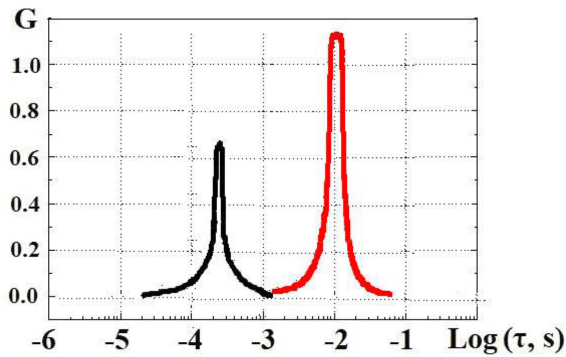

Fig. 4. Relaxation time distribution for doped VO_2 : Ni film
(experimental data processed by spectrometer)
Maximum positions: $1.6 \cdot 10^{-4}$ and $1.0 \cdot 10^{-2}$ s

Circumstance 2. The calculation by the symbolic method of the two-loop equivalent circuit [14] showed that the appearance of the calculated dielectric spectra only qualitatively coincides with the experimentally measured spectra.

Quantitative agreement can be achieved by analyzing a much more complex equivalent circuit with distributed electrical parameters, which dramatically complicates the calculations without introducing qualitative novelty. Therefore, we have assumed that the main features of the dielectric spectra are adequately described by the two-loop electric equivalent circuit. Thus, according to the calculation by the symbolic method, the shape of the features of the CC diagram does not depend on the conductivity of the sample, but depends only on its electrical capacitance. And since the shape of CC diagram, as the experiment shows, does not depend on temperature, changes of tg(f) function with temperature are determined for VO_2 : Ni only by temperature course of electrical resistance of nanocrystallites, but not by course of their electrical capacity (taking into account that $f = 1/2\pi = 1/2\pi RC$).

Interpretation of experimental results. It is based on a number of considerations, as follows.

1. The maximum of the function $\varepsilon''(f)$ resulting from the doping of a film with unimodal crystallite size distribution is located for the VO_2:Ni film on the high-frequency side from the main maximum due to undoped grains of the material. This fundamentally distinguishes this situation from the variant of undoped vanadium dioxide film with a bimodal distribution, whose dielectric spectra also contain two maxima, of which the smaller maximum is located on the low-frequency side of the main one.

2. The metallic bonding energy of nickel (430 kJ/mol) is 25% lower than that of vanadium (520 kJ/mol) (see Table 1). This means, first, that the thermodynamic potential minimization condition causes the surface of the smallest nanocrystallites to become saturated with clusters of metallic nickel rather than vanadium, as in an undoped vanadium dioxide film with a bimodal size distribution of nanocrystallites. Secondly, it means that in the case of doped VO_2:Ni films there is no continuous nickel metallization of the grain surface, which ensures free access of oxygen deep into the grain during synthesis, since the nickel concentration is only 1 molar %. Thirdly, the condition of minimizing the surface energy dictates the formation of the smallest crystallite surface (but not in their volume) of metallic nickel clusters with multi-electron metal bonding, whose energy is much lower than the two-electron bonding energy of dimer Ni-Ni or bonds Ni-O (we discuss details of the mechanism of difference in

bond energy below). It follows that the thermal hysteresis loops of the features due to doping have to be, because of martensitic properties, substantially wider than for the bimodal undoped case.

3. The above arguments allow us to state that throughout the crystallite thickness proper stoichiometry must be observed and the volume of vanadium dioxide crystallites must be doped with Ni^{4+} ions, which substitute V^{4+} ions in the centers of oxygen octahedrons, creating six σ-bonds with oxygen ions each. In this case each Ni^{4+} ion replacing V^{4+} is in the next electron hybridization state:

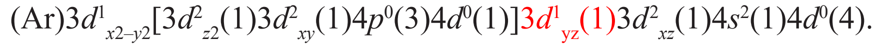

$$(Ar)3d^1_{x2-y2}[3d^2_{z2}(1)3d^2_{xy}(1)4p^0(3)4d^0(1)]3d^1_{yz}(1)3d^2_{xz}(1)4s^2(1)4d^0(4).$$

For comparison, here is the electron hybridization of the V^{4+} ion, which has a similar electron level system structure:

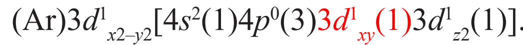

$$(Ar)3d^1_{x2-y2}[4s^2(1)4p^0(3)3d^1_{xy}(1)3d^1_{z2}(1)].$$

4. By replacing the V^{4+} ion in the center of the octahedron, the Ni^{4+} ion would have to form Ni-V dimers due to the formation of σ-bonds of $3d^1_{x2-y2}$ orbitals of Ni^{4+} ions and the same orbitals of V^{4+} ions of neighboring octahedrons containing one electron each. However, the $3d^1_{yz}$ orbital not participating in the formation of the crystal frame (highlighted in the Ni^{4+} electron configuration line) also contains one electron, which cannot remain free inside the crystal lattice. Therefore, inside the VO_2 lattice when doped with nickel, Ni-Ni dimers arise due to the double bonds. Namely, by σ-bonding the $3d^1_{x2-y2}$ orbitals of Ni^{4+} ions to neighboring octahedrons and π-bonding the $3d^1_{yz}$ cross-shaped orbitals of the same Ni^{4+} ions in neighboring octahedrons.

5. The bonding energies of these dimers, according to the Pauling mechanism [7], are greatly underestimated compared to the energies of the V-V-dimers. The fact is that during the formation of the crystal frame three orbitals are outside the oxygen octahedron with the Ni^{4+} ion at its base center (as follows from the analysis of the Ni^{4+} electronic hybridization). All these orbitals are occupied by electrons unlike the V^{4+} ion in the vanadium dioxide framework, which is not doped with nickel. It is important that the nearest electron-free orbital not involved in hybridization is the $4d^0$ orbital, which is essentially necessary to allow the formation of the conduction band π*. This situation arises because the *d*-shell of the nickel atom differs from the *d*-shell of the vanadium atom: the under-populated *d*-shell of the nickel atom has no electron-free orbitals. For example, nickel has 8 electrons on the five *d*-levels, which, according to Hund's first rule, occupy all orbitals, three of which have 2 electrons each. And the donor-acceptor π-bonds $4d^0{-}2p^2_z$ with oxygen ions located in the corners of the octahedron bases form empty $4d^0$-orbitals (similar to the situation with V^{4+} ions). These bonds in the VO_2:Ni crystal are necessarily included in the formation of the energy position of the π- and π*-bands (similar to the $3d^0{-}2p_z$ π-bonds for vanadium). The π*-energy zone in both cases plays the role of a conduction zone [3]. The energy gap between the bonding (π) and antibonding (π*) zones for the $4d^0{-}2p^2_z$ π-bond of Ni^{4+} ion is smaller than for the $3d^0{-}2p_z$ π-bond of V^{4+} ion, according to the above mentioned Pauling mechanism [7]. The mechanism is reduced to the fact that the energy of those chemical bonds whose orbitals are more strongly shielded by the inner electron shells is lower. It follows that doping with nickel ions decreases the band gap width of the doped VO_2:Ni film in proportion to the concentration of nickel ions, because more electrons are involved in bond shielding for this ion than for V^{4+}.

The $3d^1_{x2-y2}$ and $3d^1_{yz}$ orbitals participate in the formation of Ni-Ni dimers in the same way as in the formation of V-V dimers in undoped vanadium dioxide. However, the binding energy of Ni-Ni dimers, according to the same rule of Pauling, is again much lower than that of the dimer V-V, due to shielding the orbitals of bonds Ni-Ni additional (relative to the vanadium atom) with five electrons of the *d*-shell. The nickel atom 3*d*-shell contains eight electrons instead of three in the vanadium atom. The $4s^2$ orbital, as well as the $3d^2_{xz}$ orbital, being fully saturated, in the first approximation does not participate in electron transfer into conduction band, like the fully saturated $2p^2_z$ orbital of the oxygen atom, and forms inside of crystal lattice an undivided electron pair [22].

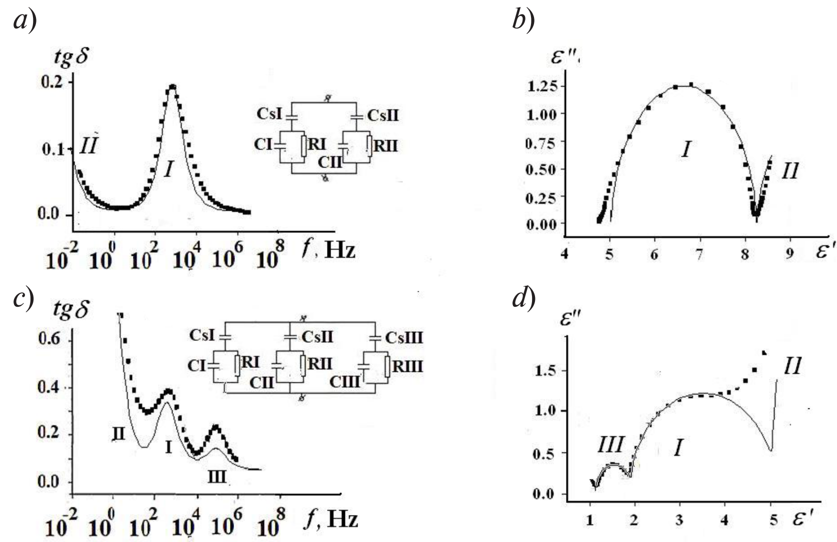

Fig. 5. Comparison of frequency dependences of tgδ(*f*) and CC diagrams for undoped VO_2 film (*a, b*) and tungsten-doped VO_2 : W film (*c, d*) at T = 293 K (points correspond to the experiment, solid lines to the calculation result)
The values of parameters of the elements of equivalent circuits are presented in Table 2

Table 2

Equivalent circuit parameter values for undoped and doped VO_2 films (see Fig. 5)

Parameter	Marking on the schemes	Parameter value for film	
		VO_2	VO_2 : Ni
Capacitance, pF	CI	35	22
	CII	100	30
	CIII	–	500
	CsI	10	60
	CsII	35	25
	CsIII	–	70
Resistance, MOhm	RI	1,5	1500
	RII	10^5	0,07
	RIII	–	1500

The following conclusions can be drawn from the statements above.

I. The positions of both maxima of the function ε″(*f*) on the temperature scale of the thermal hysteresis loops indicate a Peierls PT semiconductor-metal in a pattern typical for vanadium dioxide films. The phase equilibrium temperature of films (334 K (61 °C)) is always a few degrees below that of bulk vanadium dioxide single crystals (340 K (67 °C)), due to the presence of small defects of nanocrystallites in the form of oxygen vacancies, inevitably occurring during synthesis [20]. We remind you that the hysteresis loop of bulk vanadium dioxide monocrystals has a width of 1 K and strictly vertical branches.

II. The widths of hysteresis loops of both maximums of doped VO_2 : Ni film are many times greater than those of bulk VO_2 monocrystals, and the branches of the loops have a slope depending on the half-width of film crystallite size distribution due to martensitic character of PT.

2.4. Tungsten-doped VO_2 film

Importantly, $V_{1-x}W_xO_2$ epitaxial films 900 ± 50 E thick were synthesized on rutile substrates by laser ablation of vanadium and tungsten metal targets with oxidation of the metal droplet plume in a low pressure oxygen flow [23, 24].

2.4.1. Experimental results

Fig. 5 shows frequency dependences of tgδ(*f*) as well as Cole–Cole diagrams for undoped vanadium dioxide film and tungsten-doped W (VO_2:W) film. Comparison of dielectric spectra of doped film (Fig. 5, c, d) with spectra of undoped film (Fig. 5, *a*, *b*) shows that the frequency dependence tgδ(*f*) for VO_2:W film at T = 293 K exhibits three maxima instead of two, and, besides, the structure of CC-diagram is complicated. The latter has three semicircles according to the number of maxima of the tg(*f*) function, although the semicircle of the largest diameter is represented only partially because of the limited frequency range of the spectrometer. The frequency of maximum III, generated by doping, appeared to be two orders of magnitude higher than the frequency of the main maximum I of the spectrum of undoped film.

Equivalent circuit diagrams of the samples. The analysis of the experimental curves is based on a two-loop and three-loop equivalent circuit. The insets to Fig. 5, *a*, *c* show circuits containing complexes of two or three loops connected in parallel with each other. The physical meaning of the elements of the suggested schemes is the following: capacities CI, CII are electrical capacities of undoped VO_2 grains aggregates, and CIII is the capacity of doped VO_2 : W grains (C_0 is empty cell capacity, C_0 = 22 pF, it was used in calculations but is not presented in schemes); RI, RII and RIII are averaged electrical resistances of corresponding aggregates of grains. The capacitances CsI, CsII and CsIII are the total electrical capacitances of those three parts of the substrate on which grains of the three aggregates with different physical properties are placed in random order.

The calculation of the three-loop circuit is done symbolically using standard computer programs. The calculation allows numerical solutions for both the tgδ(*f*) relation and the ε″(ε′) diagram. Fig. 5 shows the results of this calculation as solid curves, and they are in good agreement with the measurement results (dots). The good agreement confirms the validity of the proposed equivalent schemes. Numerical values of equivalent circuit parameters are shown in Table 2.

Temperature dependencies of DS features. The temperature hysteresis loop of the frequency position of the main maximum f_0I corresponds to a set of undoped film grains and corresponds to the temperature of the structural PT T_C = 340 K (67 °C). The loop of frequency position of the second maximum f_0II can be measured only partially, as its position is outside the frequency interval of the spectrometer. The frequency position loop of the third maximum f_0III which is connected in dielectric spectra with the doping of VO_2 film with tungsten is located at temperature T_C = 320 K (47 °C), which corresponds to the thermal hysteresis loop of conductivity of VO_2 : W film (Fig. 6), its middle point corresponding to the phase equilibrium temperature is also located at lower temperature T_C = 320 K.

Let us point out a number of features of the hysteresis loops of VO_2 : W films.

a) Tungsten doping lowers the T_C temperature by 28 K.

b) The doping narrows the loop from 10 to 7 K.

c) Tungsten doping generates non-parallelism of the heating and cooling branches of the loop.

d) Doping results in loops with sharply asymmetric high temperature and low temperature regions.

e) Tungsten doping shortens the length of the high-temperature region of the loop.

These features are relevant when analyzing the dielectric spectra of doped VO_2 : W films.

Firstly, the long and narrow high-temperature "beak" loop of the undoped film suggests a relationship between T_C phase equilibrium temperatures and elementary loop widths for the largest crystallites with narrow loops (which is quite common in the property behavior of vanadium dioxide [25]).

Secondly, the reason for this dependence is the strong bond between the vanadium dioxide nanocrystallites and the TiO_2 rutile substrate, which provides a large elastic strain energy storage during lattice transition from the monoclinic to the tetragonal phase and returns this energy to the lattice when cooling.

Third, the crystal-substrate interaction process is most effective for a small population of the largest grains that have the largest contact area with the substrate. In this population, the phase transition forms the high-temperature apex of the hysteresis loop.

Fourthly, tungsten doping weakens the bonding of crystallites to the substrate because of the much larger spatial extent of the tungsten orbitals than vanadium. This weakening is due to the saturation of the contact area with the substrate by tungsten ions and the adhesion bonds it creates have less energy than vanadium bonds (according to the Pauling mechanism (see above)).

Fifthly, this weakening of the bond is manifested by a decrease after doping in the thermal extent of the upper 'beak' of the loop and in the appearance of non-parallelism of the loop branches (see Fig. 5,*b*); besides, a fragment of the fourth semicircle of the CC diagram appears in the area related to high frequencies (left from the center of the large semicircle). The reason for the appearance of this fragment is the outstripping growth of the electron concentration in the contact layer between the crystal and the substrate due to the destruction of the adhesion bonds weakened by the tungsten shielding.

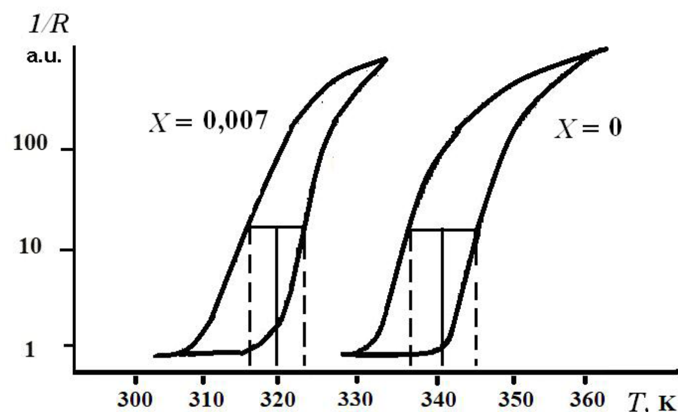

Fig. 6. Demonstration of change in shape and position of thermal hysteresis loop of conductivity of $V_{1-x}W_xO_2$ films when doped with tungsten: $x = 0$ and $x = 0.007$

2.4.2. Interpretation of results

In the doping of vanadium dioxide with tungsten the W^{4+} ion replaces the V^{4+} ion, giving up four electrons to form six hybrid orbitals and gaining the valence 4+. The W^{4+} ion in this case behaves in the lattice of vanadium dioxide like the V^{4+} ion, and in the semiconductor phase, it is able to form a dimer W-W like a pair of Ni-Ni and V-V. However, unlike the V^{4+} ion, the W^{4+} ion, as well as the Ni^{4+} ion, has an additional electron on one of the remaining *d*-orbitals, which do not participate in the hybridization; this electron cannot remain in the lattice without interaction. This results in the formation of W-W dimers bonded by a double bond.

Donor properties of tungsten ion at electron transfer into conduction zone π^* play an important role in the process of lowering the temperature of T_C phase transition, which is caused by strong correlation effects leading to lowering of conduction zone π^* energy at its occupation by electrons.

However, the process of reducing the T_C temperature when doped with such a massive atom as tungsten has its own peculiarities which require more detailed analysis. The appearance of the third maximum in the dielectric spectrum must also be explained. Let us consider these issues in more detail.

The electron configuration of a neutral W atom is:

$$(\mathrm{Kr})4d^{10}(5)4f^{14}(7)5s^2(1)5p^6(3)\underline{5d^4(5)}5f^0(7)6s^2(1)6p^0(3)6d^0(5).$$

Highlight the configurations of the upper electron shells (5th and 6th):

$$5s^2(1)5p^6(3)[\underline{5d^1_{xy}(1)5d^1_{z2}(1)6s^2(1)6p^0\,(3)}],$$

$$\underline{\{5d^1_{x2-y2}(1)\}\ \{5d^1_{yz}(1)\}}\ 5d^0_{xz}(1)\ 6d^0(5).$$

The orbitals in square brackets (highlighted in bold and underlined) create six hybrid orbitals that ensure the integrity of the crystal framework through σ-bonds with the oxygen ions of the O^{2-} octahedron. Let the reader note that both bracketed 5*d*-orbitals contain one electron each. In this case the $5d^1_{x2-y2}(1)$ orbital could create W-V dimers similar to the V-V dimers of the undoped film. But the presence of another orbital, namely $5d^1_{yz}(1)$ with one free electron, determines, as in the case of nickel doping, the creation of W-W dimers held by double bonds: σ-bonded $5d^1_{x2-y2}(1)$ orbitals and π-bonded $5d^1_{yz}(1)$ cross-like orbitals. The situation here is similar to that with Ni-Ni dimers in VO_2 : Ni film, but with the essential difference that in VO_2:W film the doping leads to an additional maximum in dielectric spectra at extremely low frequencies (see Fig. 5).

This picture is similar to that of the dielectric spectra of an undoped vanadium dioxide film with a bimodal crystallite size distribution. The reason for the similarity is that ensuring the necessary mobility of the extremely heavy tungsten atom forces the synthesis process to use an increased substrate temperature, which, as indicated, is 650 °C. This inevitably gives rise to a significant number of small-sized crystallites with a vanadium-metallized surface, similar to the bimodal variant of undoped vanadium dioxide. The reasons for the location of the maximum in the spectra of metallized grains at extremely low frequencies are described in more detail in section 3, describing the bimodal size distribution of crystallites. The only difference is that the height of the additional maximum of the dielectric loss tangent tg(δ) spectrum (the maximum is due to the tungsten) is very large due to the large energy losses due to the large mass of the tungsten atom.

Before we explain the more effective lowering of the T_C temperature with tungsten alloying compared to that with light dopants, we note the following.

According to the Pauling mechanism (see section 2.4.2 above), due to the screening by the inner shells, the bonding energies of the W-W dimers are greatly reduced compared to those of the V-V dimers. This increases their thermal fracture efficiency many times that of the V-V or Ni-Ni bonds of the corresponding dimers. In addition, analysis of the electronic hybridization of tungsten shows that $5d^1_{x2-y2}(1)$, $5d^1_{yz}(1)$, and $5d^0_{xz}(1)$ orbitals are not involved in the construction

of the crystal framework. Two of them are occupied by electrons and the third is free. The non-participation in hybridization of the nearest $5d^0_{xz}(1)$ and $6d^0(5)$ orbitals, which are free of electrons, plays a fundamental role. These vacant $5d^0$- and $6d^0$-orbitals form donor-acceptor π-bonds $5d^0{-}2p^2_z$ and $6d^0{-}2p^2_z$ z with oxygen ions situated in the corners of the octahedron bases (similar to the corresponding structures with V^{4+} ions). These bonds are included in the formation of the energy position of the zones π and π* (similar to the $3d^0{-}2p_z$ π-bonds for vanadium octahedrons). In this case the π*-energy zone in vanadium dioxide plays the role of a conduction zone [3]. The energy gap between the bonding (π) and opening (π*) zones, due to shielding by inner shells, is substantially lower for the π-bond $5d^0{-}2p^2_z$ than for the π-bond $3d^0{-}2p_z$ of V^{4+} ion (let alone π-bond $6d^0{-}2p^2_z$), according to the same Pauling mechanism [7]. In a crystal, both of these bonds involved in the formation of zones π and π*, lead to the fact that the doping with tungsten ions reduces the band gap width VO_2:W in proportion to the concentration of tungsten ions, due to the previously described shielding the inner shells of donor-acceptor bonds $5d^0{-}2p^2_z - \pi$ and $6d^0 - 2p^2_z - \pi$.

Finally, a few words about the relaxation time distribution function.

In accordance with the presence of three maxima in the dielectric spectra, the three circles in the CC diagram and the eligibility of the three-loop equivalent electrical circuit, we can conclude that the function for the complex permittivity must be

$$\varepsilon^*(\omega) = \varepsilon_\infty + \frac{\Delta\varepsilon_1}{1+i\omega\tau_1} + \frac{\Delta\varepsilon_2}{1+i\omega\tau_2} + \frac{\Delta\varepsilon_3}{1+i\omega\tau_3}.$$

Fitting the calculation results to experimental data gives the following numerical values of relaxation times for the three types of relaxators: $\tau_1 = 1$ s, $\tau_2 = 2\cdot10^{-4}$ s, $\tau_3 = 1.6\cdot10^{-6}$ s.

Conclusion

In this work thin nanocrystalline films of a strongly correlated material, vanadium dioxide, were investigated by dielectric spectroscopy. Both specially undoped vanadium dioxide films and vanadium dioxide films doped with nickel and tungsten were fabricated and tested beforehand. The processing, analysis and interpretation of the experimental data led the authors for the first time to the following conclusions.

It is shown that in both doped and un-doped vanadium dioxide nanocrystalline films the values of parameters of dielectric spectra (frequency position of steps $\varepsilon'(f)$, position and shape of maxima $\varepsilon''(f)$ and $\mathrm{tg}\delta(f)$, form and position of a semicircle in the Cole-Cole diagram, features of function HN) are caused by the concrete type of relaxators, namely free electrons, for which the dielectric response speed is defined by various times of a Maxwell relaxation $\tau_M = \varepsilon\varepsilon_0/\sigma$.

It was found that for a set of undoped nanocrystalline film grains the response time in the maximum of relaxator distribution over their times at $T = 293$ K is $\tau_{M1} = 10^{-2}$ s, whereas for a set of doped nickel grains the Maxwell time is two orders of magnitude shorter: $\tau_{M2} = \tau_2 = 1.6\cdot10^{-4}$ s.

It is shown that in the semiconductor phase at 20 °C, far from the Peierls phase transition temperature ($T_C = 67$ °C), the maximums of functions $\varepsilon''(f)$ and $\mathrm{tg}\delta(f)$ are situated at low frequencies, because of small specific electrical conductivity of nanocrystallites of the film, which corresponds to a large Maxwell relaxation time $\tau = \varepsilon\varepsilon_0/\sigma$.

It is shown that because of the realization of the Pauling mechanism the electron concentration in the group of nickel-doped vanadium dioxide film grains is higher at any temperature than in the unalloyed ones. This determines the location of maximums of functions $\varepsilon''(f)$ and $\mathrm{tg}\delta(f)$ for nickel-doped crystallites in higher frequency region of dielectric spectra ($f_{2dop} = 1000$ Hz) than for a set of undoped grains ($f_{1undop} = 14$ Hz).

It is established that the dielectric spectrum parameters clearly indicate the increase of electrons concentration in the conduction band of semiconductor phase of VO_2 : Ni and VO_2 : W films at thermal destruction of Ni-Ni and W-W dimers, in full correspondence with the process of destruction of V-V dimers of undoped films.

It is found that before the structural Peierls phase transition, as the temperature rises by 40°C (from 20 to 60 °C), the maximum positions of the functions $\varepsilon''(f)$ and $\mathrm{tg}\delta(f)$ on the dielectric spectra are significantly displaced towards high frequencies, and relaxation times $\tau_1 = 1/(2\pi f_1)$, $\tau_2 = 1/(2\pi f_2)$ and $\tau_3 = 1/(2\pi f_3)$ are shortened on orders of magnitude, that is determined by growth

of specific conductivity σ.

It is shown that the information obtained by dielectric spectroscopy (DS) indicates a complex Mott-Peierls phase transition (PT) in the VO_2:Ni film, when the structural Peierls PT is preceded by a temperature extended electronic Mott PT. After this Peierls PT occurs, then at further temperature growth the second Mott phase transition takes place, as indicated by the DS method, demonstrating a shortening of relaxation times τ_1 and τ_2 by two orders of magnitude.

Based on the method of multi-loop equivalent circuits the possibility of the adequate mathematical description of both relaxation processes and multifactor charge transfer processes in films of strongly correlated metal compounds has been demonstrated.

The possibility has been shown to investigate selectively by DC method the peculiarities of through-current flow and details of charge accumulation processes in multi-sized sets of nanocrystallites randomly mixed on a substrate carrying a nanocrystalline film in the process of synthesis.

Thus, using dielectric spectra of thin films of strongly correlated material, vanadium dioxide, as an example, it is shown that the high sensitivity of the DS method allows one to obtain dielectric spectra of extremely thin (about 500 E) films of transition metal oxides within a wide frequency range (10^{-3} to 10^{11} Hz).

This allows us to state that the described results of dielectric spectra together with the results of studies of charge transport processes, optical properties of films and phase transformation parameters in nanocrystalline strongly correlated materials form a unified research complex. This complex is capable of delivering unique scientific information that is inaccessible to other methods and is indispensable for the design of applications based on strongly correlated materials.

Acknowledgment

The study was supported by RFBR grant 20-07-00730.

The authors declare no conflict of interest.

REFERENCES

1. **Malyshev V. I.,** Introduction to experimental spectroscopy, Nauka, Moscow, 1979 (in Russian).

2. **Shadrin E. B., Ilinskii A. V.,** On the nature of metal-semiconductor phase transition in vanadium dioxide, Physics of the Solid State. 42 (6) (2000) 1126–1133.

3. **Ilinskiy A. V., Kvashenkina O. E., Shadrin E. B.,** Correlation nature of phase transformations in nanocomposites on the basis of VO_2, Smart Nanocomposites. 4 (2) (2013) 65–74.

4. **Adaskin A. M., Sedov Yu. E., Onegina A. K., Klimov V. N.,** Materialovedeniye v mashinostroyenii [Materials technology in machine-building], in 2 Vols., 2nd ed., Part 1, Yurait Publishing, Moscow, 2019 (in Russian).

5. **Akhmetov N. S.,** General and inorganic chemistry, 2nd Ed., Mir Publishers, Moscow, 1983.

6. **Eremin V. V., Kargov S. I., Uspenskaya I. A., et al.,** Osnovy fizicheskoy khimii. Teoriya i zadachi [Fundamentals of physical chemistry. Theory and examples], “Exam” Publishing, Moscow, 2005 (in Russian).

7. **Pauling L.**, The nature of the chemical bond, 3rd Ed. Cornell Univ. Publishing, New York, 1960.

8. **Lobodyuk V. A, Estrin E. I.,** Isothermal martensitic transformations, Physics–Uspekhi. 48 (7) (2005) 713–732.

9. Dielectric measurements. In book: Fizicheskaya entsiklopediya v 5 tt, 1988 – 1998, Gl. redaktor A. M. Prokhorov, T. 1 (А – Д) [Physical Encyclopaedia, in 5 Vols., 1988–1998, Chief Editor A. M. Prokhorov, Vol. 1 (А – Д), Soviet Encyclopaedia, Moscow (1988) P. 700.

10. **Volkov A. S., Koposov G. D., Perfilyev R. O., Tyagunin A. V.,** Analysis of experimental results by the Havriliak – Negami model in dielectric spectroscopy, Opt. Spectrosc. 124 (2) (2018) 202–205.

11. **Volkov A. S., Koposov G. D., Perfilyev R. O.,** On the physical meaning of disperse parameters of frequency dependence of dielectric permittivity in the Havriliak – Negami model, Opt. Spectrosc. 125 (3) (2018) 379–382.

12. **Landau L. D., Lifshits E. M.,** Course of theoretical physics, Vol. 3. Quantum mechanics (Non-relativistic theory), 3rd edition, Butterworth-Heinemann, Oxford, UK, 1981.

13. **Gatti M., Bruneval F., Olevano V., Reining L.,** Understanding correlations in vanadium dioxide from first principles, Phys. Rev. Lett. 99 (26) (2007) 266402.

14. **Ilinskiy A. V., Shadrin E. B., Kastro R. A., Pashkevich M. E.,** Dielectric spectroscopy and features of the mechanism of semiconductor – metal phase transition in VO_2 films, Semiconductors. 54 (2) (2020) 205–211.

15. **Ilinskiy A. V., Pashkevich M. E., Shadrin E. B.,** Steπ-by-step modeling of the semiconductor-metal phase transition mechanism in vanadium dioxide, St. Petersburg State Polytechnical University Journal. Physics and Mathematics. 10 (3) (2017) 9–17.

16. **Ilinskii A. V., Kastro R. A., Pashkevich M. E., Shadrin E. B.,** Dielectric spectroscopy as a method for testing thin vanadium dioxide films, Techn. Phys. 64 (12) (2019) 1790–1795.

17. **Khakhaev I. A., Chudnovskii F. A, Shadrin E. B.,** Martensitic effects in the metal-insulator phase transition in a vanadium dioxide film, Physics of the Solid State. 36 (6) (1994) 898–901.

18. **Anisimov S. I., Lukyanchuk B. S.,** Selected problems of laser ablation theory, Physics–Uspekhi. 45 (3) (2002) 293–324.

19. **Podsvirov O. A., Vostokov A.V., Sidorov A. I., Tsekhomskii V.A.,** Formation of copper nanocrystals in photochromic glasses under electron irradiation and heat treatment, Physics of the Solid State. 52 (9) (2010) 1906–1909.

20. **Aliyev R. A., Klimov V. A.,** Effect of synthesis conditions on the metal-semiconductor phase transition in vanadium dioxide thin films, Physics of the Solid State. 46 (3) (2004) 532–536.

21. **Asabina E. A.,** Defekty v tverdykh telakh i ikh vliyaniye na svoistva funktsionalnykh materialov [Defects in solids and their influence on the properties of functional materials], The University of Nizhny Novgorod, Nizhny Novgorod, 2012 (in Russian).

22. **Nikolsky B. P.** (Editor), Chemist's handbook, Vol. 3, Khimiya, Leningrad, 1965 (in Russian).

23. **Andreev V. T., Gurvitch M. A., Klimov V. A., et al.,** Laser deposition of vanadium dioxide films, Pis'ma v Zhurnal Tekchnicheskoj Fiziki. 19 (9) (1993) 63–65 (in Russian).

24. **Andreev V. T., Chudnovskii F. A., Klimov V. A.,** Resistivity of the metallic phase of epitaxial VO_2 films, Pis'ma v ZhETF. 60 (9) (1994) 637–638 (in Russian).

25. **Vinogradova O. P., Obyknovennaya I. E., Sidorov A. I., et al.,** Synthesis and the properties of vanadium dioxide nanocrystals in porous silicate glasses, Physics of the Solid State. 50 (4) (2008) 768–774.

СПИСОК ЛИТЕРАТУРЫ

1. **Малышев В. И.** Введение в экспериментальную спектроскопию. М.: Наука, 1979. 479 с.

2. **Шадрин Е. Б., Ильинский А. В.** О природе фазового перехода металл – полупроводник в диоксиде ванадия // Физика твердого тела. 2000. Т. 42. № 6. С. 1092–1099.

3. **Ilinskiy A. V., Kvashenkina O. E., Shadrin E. B.** Correlation nature of phase transformations in nanocomposites on the basis of VO_2 // Smart Nanocomposites, 2013. Vol. 4. No. 2. Pp. 65–74.

4. **Адаскин А. М., Седов Ю. Е., Онегина А. К., Климов В. Н.** Материаловедение в машиностроении. В 2 ч. 2-е изд. Часть 1. М.: Издательство «Юрайт», 2019. 258 с.

5. **Ахметов Н. С.** Общая и неорганическая химия. 12-е издание. СПб.: Издательство «Лань», 2021. 744 с.

6. **Еремин В. В., Каргов С. И., Успенская И. А., Кузьменко Н. Е., Лунин В. Е.** Основы физической химии. Теория и задачи. М.: Издательство «Экзамен», 2005. 480 с.

7. **Полинг Л.** Природа химической связи. Москва-Ленинград: Госхимиздат, 1963. 440 с.

8. **Лободюк В. А., Эстрин Э. И.** Изотермическое мартенситное превращение // Успехи физических наук. 2005. Т. 175. № 7. С. 745–765.

9. Диэлектрические измерения // Физическая энциклопедия. В 5 тт. 1988 – 1998. Гл. ред. А. М. Прохоров Т. 1. А – Д. М.: Советская энциклопедия, 1988. 704 с. (С. 700).

10. **Волков А. С., Копосов Г. Д., Перфильев Р. О., Тягунин А. В.** Анализ экспериментальных результатов по модели Гавриляка – Негами в диэлектрической спектроскопии // Оптика и спектроскопия. 2018. Т. 124. № 2. С. 206–209.

11. **Волков А. С., Копосов Г. Д., Перфильев Р. О.** О физическом смысле дисперсионных параметров частотной зависимости диэлектрической проницаемости в модели Гавриляка – Негами // Оптика и спектроскопия. 2018. Т. 125. № 3. С. 364–367.

12. **Ландау Л. Д., Лифшиц Е. М.** Теоретическая физика: в 10 тт. Т. 3. Квантовая механика. Нерелятивистская теория. М.: Наука, 1989. 766 с.

13. **Gatti M., Bruneval F., Olevano V., Reining L.** Understanding correlations in vanadium dioxide from first principles // Physical Review Letters. 2007. Vol. 99. No. 26. P. 266402.

14. **Ильинский А. В., Кастро Р. А., Пашкевич М. Э., Шадрин Е. Б.** Диэлектрическая спектроскопия и особенности механизма фазового перехода полупроводник – металл в пленках VO_2 // Физика и техника полупроводников. 2020. Т. 54. № 2. С. 153–159.

15. **Ильинский А. В., Пашкевич М. Э., Шадрин Е. Б.** Поэтапное моделирование механизма фазового перехода полупроводник – металл в диоксиде ванадия // Научно-технические ведомости СПбГПУ. Физико-математические науки. 2017. Т. 10. № 3. С. 9–17.

16. **Ильинский А. В., Кастро Р. А., Пашкевич М. Э., Шадрин Е. Б.** Диэлектрическая спектроскопия как метод исследования тонких пленок диоксида ванадия // Журнал технической физики. 2019. Т. 89. № 12. С. 1885–1890.

17. **Хахаев И. А., Чудновский Ф. А, Шадрин Е. Б.** Мартенситные эффекты при фазовом переходе металл – диэлектрик в пленке диоксида ванадия // Физика твердого тела. 1994. Т. 36. № 6. С. 1643–1649.

18. **Анисимов С. И., Лукъянчук Б. С.** Избранные задачи теории лазерной абляции // Успехи физических наук. 2002. Т. 172. № 3. С. 301–333.

19. **Подсвиров О. А., Сидоров А. И., Цехомский В. А., Востоков А. В.** Формирование нанокристаллов меди в фотохромных стеклах при электронном облучении и термообработке // Физика твердого тела. 2010. Т. 52. № 9. С. 1776–1779.

20. **Алиев Р. А. Климов В. А.** Влияние условий синтеза на фазовый переход металл – полупроводник в тонких пленках диоксида ванадия // Физика твердого тела. 2004. Т. 46. № 3. С. 515–519.

21. **Асабина Е. А**. Дефекты в твердых телах и их влияние на свойства функциональных материалов. Нижний Новгород: Нижегородский госуниверситет, 2012. 65 с.

22. Справочник химика. Под общ. ред. Б. П. Никольского. Т. 3. Ленинград: Химия,1965. 1008 с.

23. **Гурвич М. А., Климов В. А., Хахаев И. А., Чудновский Ф. А.** Лазерное осаждение пленок диоксида ванадия // Письма в Журнал технической физики. 1993. Т. 19. № 9. С. 63–65.

24. **Андреев В. Н., Климов В. А., Чудновский Ф. А.** Температурная зависимость удельного сопротивления металлической фазы VO_2 // Письма в Журнал экспериментальной и теоретической физики. 1994. Т. 60. № 9. С. 637–638.

25. **Виноградова О. П., Обыкновенная И. Е., Сидоров А. И., Климов В. А., Шадрин Е. Б., Ханин С. Д., Хрущева Т. А.** Синтез и свойства нанокристаллов диоксида ванадия в силикатных пористых стеклах // Физика твердого тела. 2008. Т. 50. № 4. С. 734–740.

THE AUTHORS

SHADRIN Evgeny B.
Ioffe Institute of the Russian Academy of Sciences
26, Polytekhnicheskaya St., St. Petersburg, 194021, Russia
jenjasha@yandex.ru
ORCID: 0000-0002-1423-2852

ILINSKIY Alexandr V.
Ioffe Institute of the Russian Academy of Sciences
26, Polytekhnicheskaya St., St. Petersburg, 194021, Russia
ilinskiy@mail.ioffe.ru
ORCID: 0000-0002-1548-1180

CASTRO ARATA Rene Alehandro
Herzen State Pedagogical University of Russia
48 Moyka Emb., St. Petersburg, 191186, Russia
recastro@mail.ru
ORCID: 0000-0002-1902-5801

KAPRALOVA Viktoria M.
Peter the Great St. Petersburg Polytechnic University
29 Politechnicheskaya St., St. Petersburg, 195251, Russia
kapralova2006@yandex.ru
ORCID: 0000-0001-9050-4453

KONONOV Aleksey A.
Herzen State Pedagogical University of Russia
48 Moyka Emb., St.Petersburg, 191186, Russia
kononov_aa@icloud.com
ORCID: 0000-0002-5553-3782

PASHKEVICH Marina E.
Peter the Great St. Petersburg Polytechnic University
29 Politechnicheskaya St., St. Petersburg, 195251, Russia
marpash@yandex.ru
ORCID: 0000-0002-3373-4129

СВЕДЕНИЯ ОБ АВТОРАХ

ШАДРИН Евгений Борисович – *доктор физико-математических наук, главный научный сотрудник, заведующий лабораторией физики фазовых переходов в твердых телах Физико-технического института имени А. Ф. Иоффе РАН.*
194021, Россия, г. Санкт-Петербург, Политехническая ул., 26
jenjasha@yandex.ru
ORCID: 0000-0002-1423-2852

ИЛЬИНСКИЙ Александр Валентинович – *доктор физико-математических наук, старший научный сотрудник лаборатории физики фазовых переходов в твердых телах Физико-технического института имени А. Ф. Иоффе РАН.*
194021, Россия, г. Санкт-Петербург, Политехническая ул., 26
ilinskiy@mail.ioffe.ru
ORCID: 0000-0002-1548-1180

КАСТРО АРАТА Рене Алехандро – *доктор физико-математических наук, ведущий научный сотрудник, профессор кафедры физической электроники Российского государственного педагогического университета имени А. И. Герцена.*
191186, Россия, Санкт-Петербург, наб. р. Мойки, 48
recastro@mail.ru
ORCID: 0000-0002-1902-5801

КАПРАЛОВА Виктория Маратовна – *кандидат физико-математических наук, доцент Высшей школы электроники и микросистемной техники Санкт-Петербургского политехнического университета Петра Великого.*
195251, Россия, г. Санкт-Петербург, Политехническая ул., 29
kapralova2006@yandex.ru
ORCID: 0000-0001-9050-4453

КОНОНОВ Алексей Андреевич – *кандидат физико-математических наук, ассистент кафедры физической электроники Российского государственного педагогического университета имени А. И. Герцена.*
191186, Россия, Санкт-Петербург, наб. р. Мойки, 48
kononov_aa@icloud.com
ORCID: 0000-0002-5553-3782

ПАШКЕВИЧ Марина Эрнстовна – *старший преподаватель кафедры высшей математики Санкт-Петербургского политехнического университета Петра Великого.*
195251, Россия, г. Санкт-Петербург, Политехническая ул., 29
marpash@yandex.ru
ORCID: 0000-0002-3373-4129

Received 22.08.2022. Approved after reviewing 23.08.2022. Accepted 23.08.2022.
Статья поступила в редакцию 22.08.2022. Одобрена после рецензирования 23.08.2022. Принята 23.08.2022.

© Peter the Great St. Petersburg Polytechnic University, 2022